SCIENTIFIC REPORTS

OPEN

SUBJECT AREAS:
MATERIALS SCIENCE
MECHANICAL PROPERTIES
MATERIALS CHEMISTRY
BATTERIES

Received
10 July 2012

Accepted
27 September 2012

Published
19 October 2012

Correspondence and requests for materials should be addressed to X.-L.W. (xlwang@cityu.edu.hk)

# Visualizing the chemistry and structure dynamics in lithium-ion batteries by *in-situ* neutron diffraction

Xun-Li Wang[1,2], Ke An[1], Lu Cai[1], Zhili Feng[3], Stephen E. Nagler[4], Claus Daniel[3,5], Kevin J. Rhodes[3,5], Alexandru D. Stoica[1], Harley D. Skorpenske[1], Chengdu Liang[6], Wei Zhang[3], Joon Kim[7], Yue Qi[8] & Stephen J. Harris[8]

[1]Chemical and Engineering Materials Division, Oak Ridge National Laboratory Oak Ridge, TN 37831–6465, [2]Department of Physics and Materials Science, City University of Hong Kong Tat Chee Avenue, Kowloon, Hong Kong, [3]Materials Science and Technology Division, Oak Ridge National Laboratory, Oak Ridge, TN 37831, [4]Quantum Condensed Matter Division, Oak Ridge National Laboratory Oak Ridge, TN 37831, [5]Department of Materials Science and Engineering, University of Tennessee, Knoxville, TN 37996, [6]Center for Nanophase Materials Sciences, Oak Ridge National Laboratory, Oak Ridge, TN 37831, [7]Dow Kokam LLC, 2901 NE Hagan Road, Lee's Summit, MO 64064, [8]General Motors R&D Center, Warren, MI 48090.

**We report an *in-situ* neutron diffraction study of a large format pouch battery cell. The succession of Li-Graphite intercalation phases was fully captured under an 1C charge-discharge condition (i.e., charge to full capacity in 1 hour). However, the lithiation and dilithiation pathways are distinctively different and, unlike in slowing charging experiments with which the Li-Graphite phase diagram was established, no $LiC_{24}$ phase was found during charge at 1C rate. Approximately 75 mol. % of the graphite converts to $LiC_6$ at full charge, and a lattice dilation as large as 4% was observed during a charge-discharge cycle. Our work demonstrates the potential of *in-situ*, time and spatially resolved neutron diffraction study of the dynamic chemical and structural changes in "real-world" batteries under realistic cycling conditions, which should provide microscopic insights on degradation and the important role of diffusion kinetics in energy storage materials.**

High capacity batteries are an important component in the overall strategy for a secured energy future[1–3]. High power Li-ion batteries require an operating lifetime of over 5,000 cycles and 10–15 years or more in order to achieve the economic viability in battery-powered vehicles and in the future electricity infrastructure[4]. These requirements are about one order of magnitude greater than what current technology provides in small format cells (as in, for example, laptop computers and cell phones). While the electrochemical performance of a battery can be reasonably well described within the model of Newman[5], our ability to predict battery life is extremely limited because many seemingly unrelated degradation mechanisms have been identified[6]. Factors contributing to the durability of large format Li-ion batteries are complex and vary widely with different electrode materials, battery manufacturing processes, cycling rate, temperature and other operating conditions. Analysis of specific degradation mechanisms can in some cases provide a rationale for experimentally observed phenomena, but without comprehensive *in-situ* experimental data, quantitative cause-and-effect relationships between observation and degradation pathways are difficult to establish.

In many cases, degradation and failure in large format batteries start locally at inhomogeneities or weak points, rather than uniformly across the entire battery[3,7,8]. Figure 1 highlights the spatial inhomogeneity in the anode of a commercial 18650 battery after it lost a significant amount of capacity under cycling. The graphite anode suffered damage near each end cap. Close examination shows that the central region of the electrode tape is largely homogeneous, while the edge areas appear to be highly fractured with a substantial loss of capacity. The optical micrographs of samples from each region are contrasted in Figure 1. Lithiation of graphite electrodes – the $LiC_6$ phase – turns them to a golden color[9] that can be readily observed. The deteriorated region, which cannot be fully lithiated, lost 2/3 of its capacity. Similar results can be expected for large format pouch cell batteries.

There is a long history of experimental characterization of the charge-discharge process in Li-ion batteries using, for example, impedance measurements[6], laboratory X-ray diffraction[10,11], and synchrotron X-ray diffraction[12]. More recently, transmission electron microscopy[13] and nuclear magnetic resonance[14,15] have been used for

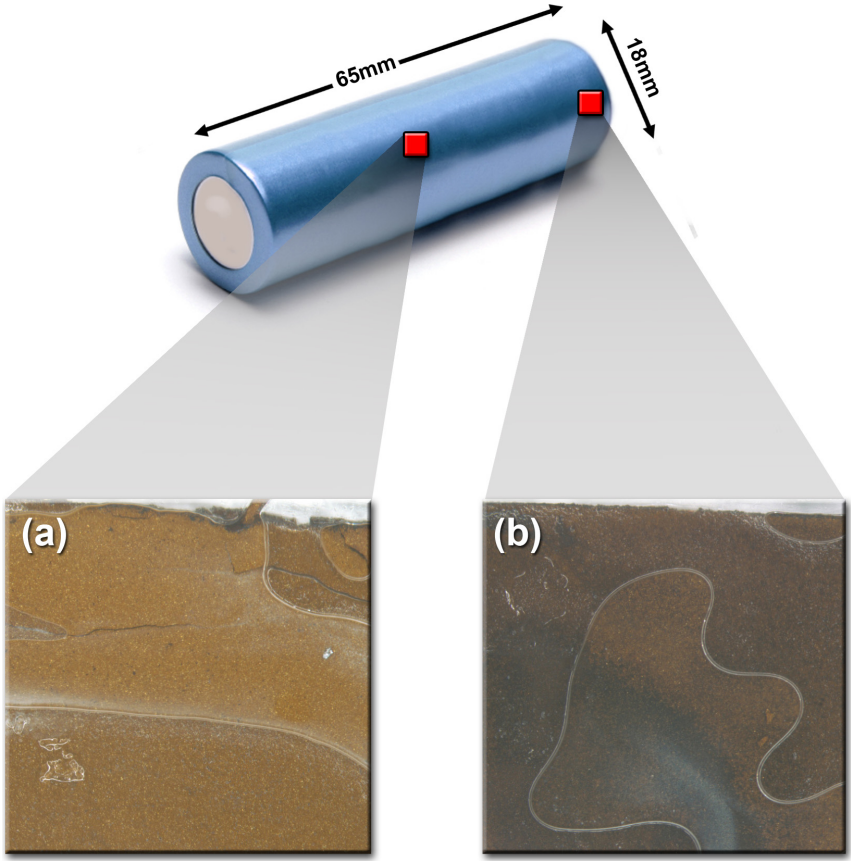


**Figure 1 | Optical micrographs taken from a failed commercial 18650 battery cells to illustrate the nature of heterogeneous failure.** The images (a) and (b), each showing a region approximately 2×2 $mm^2$ on the graphite electrode, were taken from different locations (shown as red squares). These regions were shorted to metallic Li and thereby lithiated to the maximum extent possible. Full lithiation ($LiC_6$) turns graphite to a gold color. In (a), taken far from the end caps, the entire region becomes gold, indicating that all of the graphite in this region became lithiated. In (b), taken close to the end cap (about 20 mm away from (a)) the electrode is only partially gold. Black indicates the presence of graphite particles that are not lithiated. They may have become electrically disconnected from the current collector. (The curved white lines in the images are artifacts from collecting the samples.)

*in-situ* observations. However, most of these experiments focus on small format batteries, often in half-cell form, in order to allow access to the anode or cathode material for detailed studies. As a battery's performance and service life strongly depend upon its design and packaging[16], the degradation mechanisms in large format pouch cells, representative of what is in use in the newest electrified vehicles, are expected to be very different from those in small or coin cells. For example, $Li^+$ transport in a coin cell, which has excess electrolyte, can be substantially different from that in a pouch cell. Thus, *in-situ* study of large format pouch cells is necessary in order to determine the principal factors controlling the degradation in batteries for high power applications. Because degradation and failure are spatially heterogeneous, it is also important to conduct spatially resolved measurements.

In principle, neutron diffraction is well suited for *in-situ* studies of Li-ion batteries[17–22]. Neutrons are highly penetrating, which ensures that the measurements are representative of the bulk rather than from the surface region. In addition, by defining a scattering volume using slits or collimators, as illustrated in Figure S1 of Supplemental Materials, neutron diffraction becomes a powerful tool for non-destructive volumetric (three-dimensional) mapping. The practical limit of spatial resolution is a fraction of a millimeter. A well-known application in this regard is residual stress mapping in engineering components[23]. Finally, neutron diffraction study of Li-ion batteries also benefits from the negative scattering length of Li, which creates a large scattering contrast for the intermediate phases such as $LiC_{12}$ and $LiC_6$ (see below for calculation of the diffraction structure factors). Unfortunately, these advantages are partially offset by the moderate absorption by Li and the strong incoherent scattering from H atoms in the polymer electrolyte and packaging materials, leading to a low signal to background ratio and necessitating long counting times. For this reason, prior neutron diffraction studies have been limited to ex-situ, or slow cycling rate (>25 hours for full charge or discharge), or charge-and-hold type of experiments. However, practical applications demand fast charging, where the electrochemical performance of a battery can be strongly influenced by the diffusion kinetics of Li ions, not just the energetics of the thermodynamic equilibrium phases. The role of kinetic transformation pathway was underscored recently by Malik et al. in a theoretical study of $LiFePO_4$ batteries[24].

In this paper, we report an *in-situ* time-resolved neutron diffraction study of the chemistry and structure dynamics in a large format pouch cell, representative of the type found in electrical vehicles, under a relatively fast ~1C cycling rate (0.8C to be precise, i.e., at a rate that charges or discharges the cell in 1.25 hours). The measurements were demonstrated in a spatially resolved manner, with a well-defined scattering volume located in the center of the battery. We overcame the issue of time-resolution by using the stroboscopic measurement technique[25,26].

## Results

A 40 Ah commercial pouch cell, with the dimension 190 × 206 × 7 $mm^3$, was used in this study. The battery has a $Li_xNi_yMn_zCo_{(1-y-z)}O_2$ (NMC) composite cathode and a graphite composite anode. Cu and Al foils served as the cathode and anode current collectors, respectively.

The neutron diffraction measurements were conducted using VULCAN[27], a state-of the-art engineering diffractometer at the Spallation Neutron Source[28]. VULCAN is a time-of-flight neutron diffractometer, with which a diffraction pattern over a large range of d-spacings is collected simultaneously. A sampling volume of $5\times5\times20$ mm$^3$, defined by an incident beam slit and a radial collimator, was located at mid-depth in the middle of the battery cell. A photograph of the experimental set up is shown in Figure S2 in Supplemental Materials.

For precise phase analysis, neutron diffraction patterns at fully charged (4.2 V) and discharged (2.7 V) conditions were measured for ~1 hour of counting time. The results are shown in Figure 2(a), along with Rietveld refinements for each pattern. Four phases were observed in the fully discharged condition: NMC cathode and graphite anode, plus the Al and Cu current collectors. In the charged condition, most of the graphite phase had transformed to $LiC_6$ and $LiC_{12}$, with only traces of the graphite phase remaining. An additional peak was found at ~2.05 Å, which cannot be identified with any of the above phases, but it remained unchanged during charge and discharge.

*In-situ* neutron diffraction patterns collected during cycling are presented in Figure 2(b). Continuous acquisition of neutron diffraction data was carried out using an event-mode data acquisition[29,30] system over the course of ~20 hours during which time the battery was cycled through 7 charge-discharge sequences. The data was binned into diffraction patterns corresponding to 2.5 minutes duration, and these were strobscopically averaged[25,26] over the 7 charge-discharge cycles. More details of event-based data acquisition and stroboscopic averaging are given in Supplemental Materials. Despite averaging over 7 cycles (i.e., 17.5 min in total counting time), the statistical quality of each data set was inadequate for full Rietveld refinement of the complex diffraction patterns. A possible reason for the inadequate data is that the 7 cycles, over which the data were averaged, may not be identical. A slight difference in the charge or discharge cycles can lead to blurring or degradation of the diffraction data. Nevertheless, it is possible to utilize strong characteristic

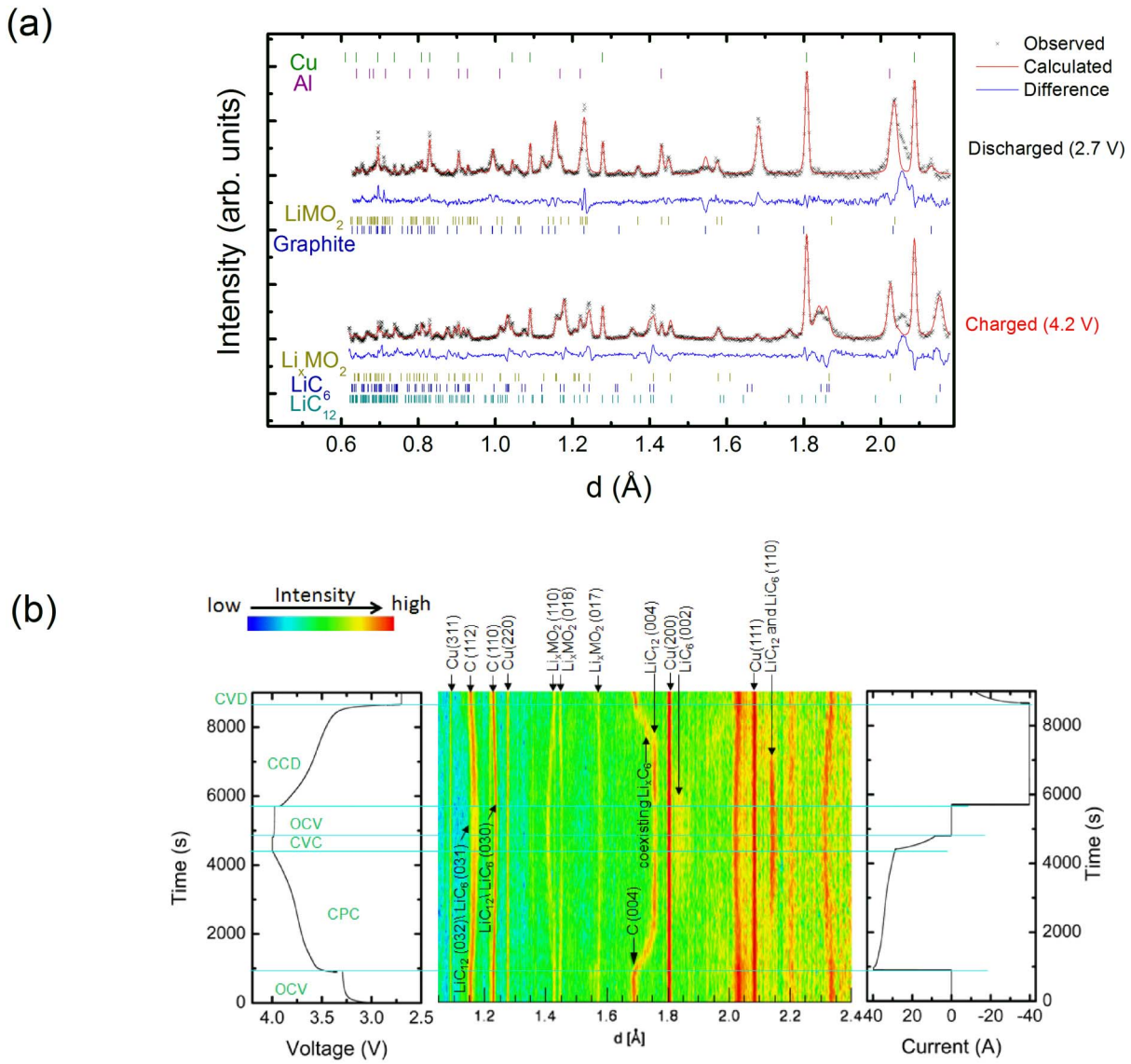


**Figure 2** | (a) Neutron diffraction patterns obtained at charged (4.2 V) and discharged (2.7 V) conditions along with the results of Rietveld refinement. (b) *In-situ* neutron diffraction pattern during a charge and discharge cycle. The *in-situ* diffraction data, averaged over 7 cycles, are binned into 2.5 minutes histograms. The voltage (current) is plotted in the side panel to the left (right) of the diffraction data. The acronyms used in the figure are as follows: CVD-constant voltage discharge, CCD-constant current discharge, OCV open circuit voltage, CVC-constant voltage charge, and CPC-constant power charge.

diffraction peaks to highlight the structural evolution in the graphite anode and NMC cathode during the charge-discharge cycles. The results are shown in Figures 3–4.

## Discussions

To facilitate discussions, we list in Table 1 the space group, lattice parameters, and stacking sequence for the graphite and pertinent Li intercalation phases[11,31–34]. The corresponding structures are shown in Figure S3 of Supplemental Materials. Graphite is made of alternating layers of graphene in ABABAB stacking sequence. During charging, Li ions intercalate between graphene layers, subsequently forming $LiC_{24}$, $LiC_{12}$, and $LiC_6$ phases with different stacking sequences between graphene and ordered Li layers. A direct consequence of lithiation in graphite is an increase of the interplanar spacing between graphene layers, a phenomenon widely used to identify phases in X-ray studies of lithiation in graphite[10,11].

From intensity point of view, the appearance of (0 0 *l*) type of peaks at distinct lattice spacings signifies the formation of the Li intercalation phases. In addition, for $LiC_{12}$ and $LiC_6$, the (1 1 0) peaks start to develop. The neutron diffraction structure factor for the $LiC_6$ (1 1 0) peak is given by $F=3b_C-b_{Li}$, where $b_C$ and $b_{Li}$ are the neutron scattering lengths for C and Li, respectively. For neutron diffraction, the (1 1 0) peak is particularly pronounced, as $b_{Li}$ is negative, leading to a large scattering contrast and hence a significantly higher diffraction intensity. Similarly, for $LiC_{12}$ (1 1 0), $F=6b_C-b_{Li}$ Note that the (1 1 0) peaks for $LiC_{12}$ and $LiC_6$ (separated by $\Delta d/d\sim0.4\%$) could not be resolved in the present experiment, probably due to their intrinsic broadening, and, as a result, they appear as one broad peak whose intensity characterizes the development of both phases. The appearance of the $LiC_6$ phase is identified by its (0 0 2) peak, which has a unique lattice spacing.

Figure 3(a) shows the evolution of lattice spacing for (0 0 *l*) peaks of graphite and various Li intercalation phases. During initial charging, the lattice spacing of the graphite (0 0 4) increased as soon as a current was applied, and reached a maximum value of 1.76 Å, or 4% expansion, after 12.5 Ah or ~2400 s of charge. The 1.76 Å interplanar spacing is characteristic of $LiC_{12}$ (0 0 4), see Table 1. Meanwhile, the intensity plot, Figures 3(b–c), shows that the (1 1 0) peak of $LiC_{12}$

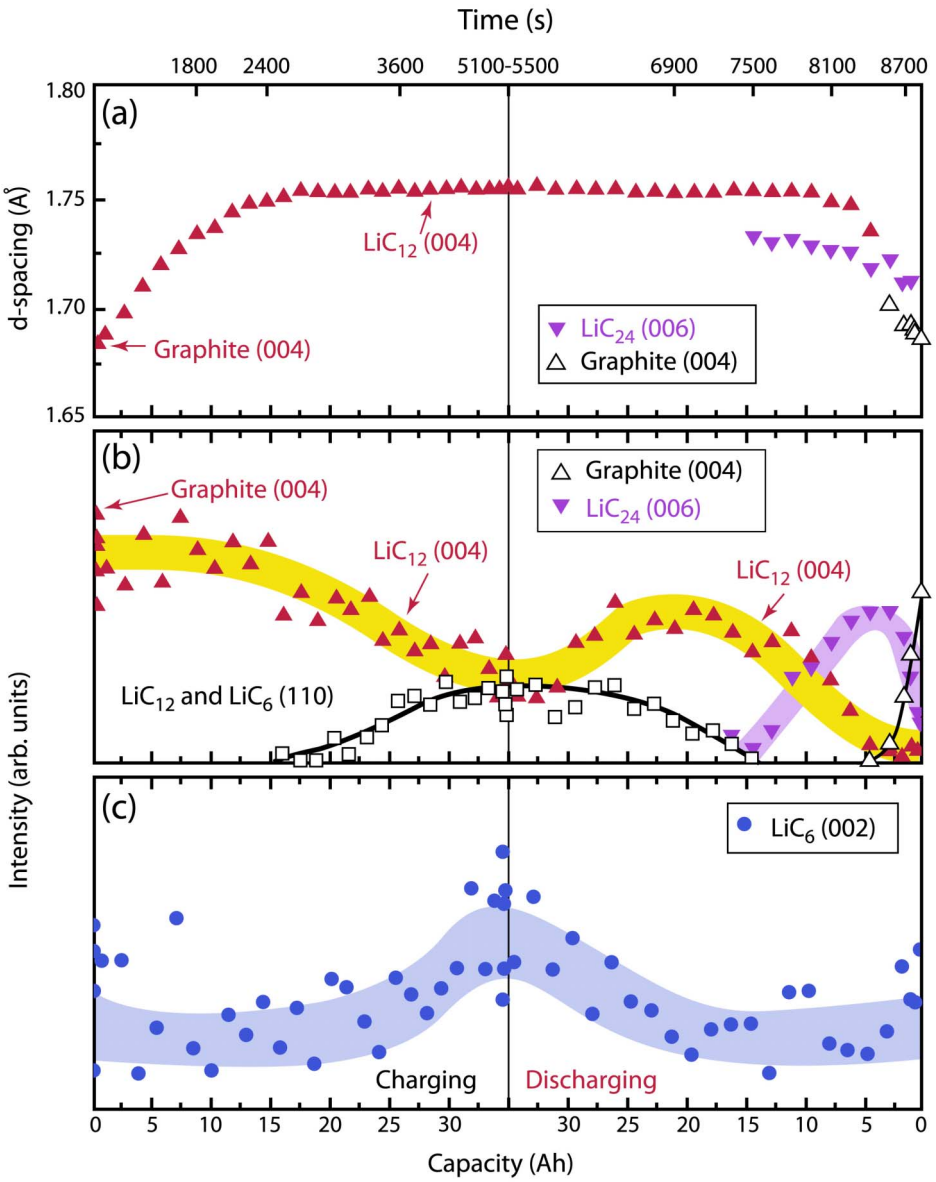


**Figure 3** | (a) Experimentally determined lattice parameters for (0 0 *l*) type of reflections for graphite and various Li graphite intercalation phases. (b) Intensity evolution of (0 0 *l*) type of reflections and the (1 1 0) peak of $LiC_{12}$ and $LiC_6$ phases. The bands are guides to the eyes. Arrows indicate the start of phase transformations.

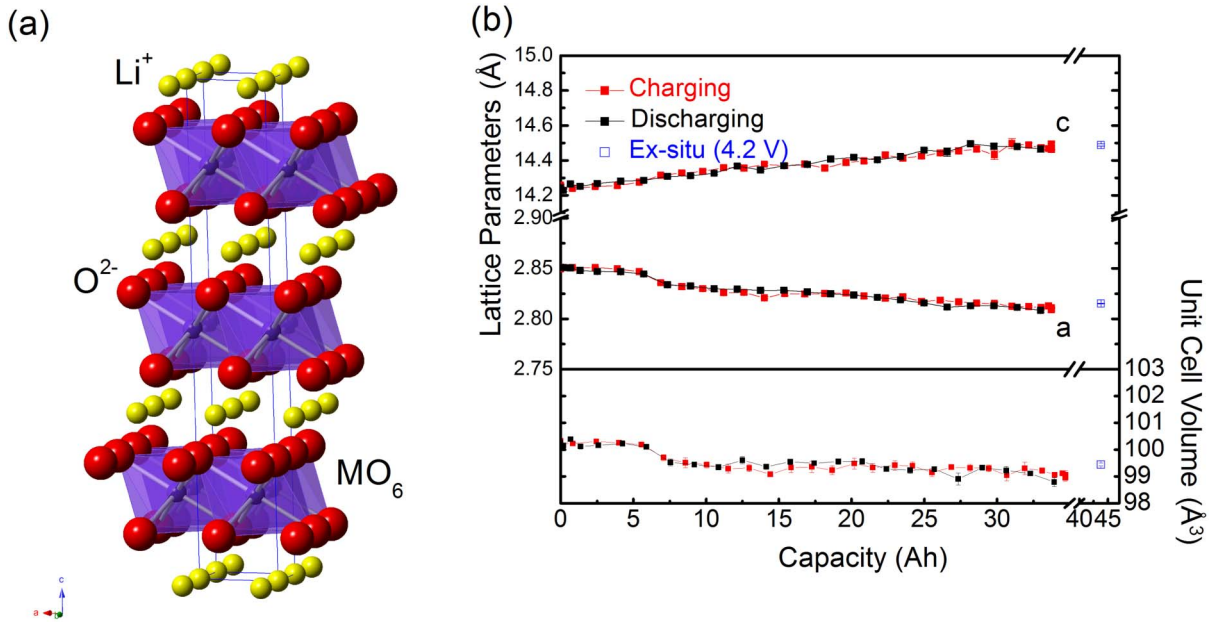


**Figure 4** | (a) The crystal structure of $Li_xNi_yCo_zMn_{(1-y-z)}O_2$ NMC cathode. The blue line indicates the unit cell. The Ni, Mn, and Co atoms are randomly distributed on M sites. (b) Change of lattice parameters and the unit-cell volume of the NMC cathode phase during a charge and discharge cycle.

(no $LiC_6$ visible yet, see below) began to develop when the lattice spacing reached its asymptotic value of 1.76 Å. This indicates that Li ions between graphene layers became ordered, forming $LiC_{12}$. At about 25 Ah or 3600 s, the $LiC_6$ (0 0 2) peak appeared, see Figure 3(c), indicating the start of $LiC_{12} \rightarrow LiC_6$ transformation. The amount of $LiC_6$ reached a maximum when the battery approached full charge, as evidenced by the intensity change of $LiC_6$ (0 0 2).

During discharge, $LiC_6$ transformed back to $LiC_{12}$ until about 20 Ah or 6900 s, when a new peak at ~1.73 Å began to develop. The lattice spacing of this peak matches that of $LiC_{24}$ (0 0 6) and is considered a signature of the $LiC_{24}$ phase. Eventually the $LiC_{24}$ phase disappeared and the graphite phase returned. The co-existence of two-phase regions (between $LiC_{12}$ and $LiC_{24}$, and between $LiC_{24}$ and graphite) can also be readily seen in the plot of lattice spacing in Figure 2(a).

There is a clear contrast between the charge and discharge cycles. Little $LiC_{24}$ (as indicated by the appearance of a peak at ~1.73 Å) or other co-existing phases were found during the charge cycle in the present experiment. This observation does not agree with the established Li-Graphite phase diagram, in which $LiC_{24}$ and graphite co-exist over a wide composition range during initial charging[10,35]. It is important to note, however, that the Li-Graphite phase diagram was established by slow charging experiments lasting up to hundreds of hours, in contrast to the rapid charge in ~1 hour as in this experiment. The near absence of $LiC_{24}$ during charging is likely due to the slow diffusion of Li ions in graphite. Using highly orientated pyrolytic graphite, Persson et al. showed that while the diffusivity of Li ions is inherently high between graphene planes, it is orders or magnitudes slower in the direction perpendicular to the planes and along grain boundaries[36]. The sluggish diffusion leaves Li ions insufficient time to sample the thermodynamic equilibrium during fast charging. Defects or disorder in the graphite anode could also trap Li ions[11], limiting its transport and therefore suppressing the formation of some of the Li intercalation phases. A closer examination of Figure 2(b) shows that, while charging, the graphite (0 0 4) peak becomes diffused which suggests the formation of a small amount of $LiC_{24}$. However, the difference between charge and discharge curves at d~1.73 Å is evident. In a separate experiment performed at a slower 0.1C cycling rate, a two-phase region was observed for a brief period during charge, indicating that cycling rate indeed plays a role. This intrigue kinetic effect apparently depends on the chemistry. For example, the kinetic effect is noticeably missing during intercalation of potassium (K) in graphite[37], induced by pressure over a wide range of pressurization rate, which authors suggest that K intercalation is nucleation rather than diffusion controlled. On the other hand, first-principles calculations identified a single-phase transformation path in $LiFePO_4$, which the authors suggest is responsible for the remarkable rate capacity of $LiFePO_4$ based batteries[24].

The fractions of the $LiC_{12}$ and $LiC_6$ phases can be calculated from Rietveld analysis of the diffraction pattern shown in Figure 2(a) at

Table 1 | Crystallographic information of graphite, $LiC_{12}$, and $LiC_6$[10,11,31–34] The structure of $LiC_{24}$ has not been fully established, but the c lattice parameter was determined to be 1.73 Å in a systematic study by Dahn[11]

| Phases | Space group | Lattice parameters (Å) | Stacking sequence* |
|---|---|---|---|
| Graphite | $P6_3/mmc$ | a = 2.464, c = 6.711 ref. 33<br>a = 2.460(2), c = 6.729(1)+ | ABABAB… |
| $LiC_{12}$ | P6/mmm | a = 4.288, c = 7.066 ref. 32<br>a = 4.290(2), c=7.047(6)+ | AAαAAα… |
| $LiC_6$ | P6/mmm | a = 4.305, c = 3.706 ref. 31<br>c = 3.700 ref. 11<br>a=4.0307(6), c=3.680(1)+ | AαAαAα… |

*A and B are graphene layers. The αs are Li ion layers.
+This work.

fully charged condition (4.2 V). Little graphite phase remained at 4.2 V, indicating that all graphite had been converted to Li interacted compounds. The refinement shows 25 mol.% of $LiC_{12}$ vs. 75 mol.% of $LiC_6$. Thus, the $LiC_{12} \rightarrow LiC_6$ conversion is incomplete even in the fully charged condition at 4.2 V. Since the $LiC_{12} \rightarrow LiC_6$ conversion is dictated by Li concentration, the incomplete transformation shows that Li ions in the cathode had all been exhausted in the fully charged condition. By definition, the state of charge, or capacity of the battery, is approximately 75% of the theoretical value for graphite.

Over the course of a full cycle, the active cathode material also undergoes a structure change. The NMC cathode has a layered $Li_xMO_2$ type of structure, with a space group of *R-3m* and lattice parameters of a ~2.8 Å and c ~14 Å[22]. The transition metal ions Ni, Mn, Co (indicated in Figure 4(a) as M in random substitution) are located at the center of oxygen octahedra. These $MO_6$ octahedra are edge-shared, forming a vertical slab parallel to the (0 0 1) planes. The $Li^+$ ions are located between the $MO_6$ slabs. The most significant structure change in NMC was the lattice dilation. The lattice parameters for NMC were obtained from analysis of diffraction peaks over d-spacings of 1.3–1.6 Å, comprising Cu (2 2 0) and NMC (1 1 3), (1 1 0), (0 1 8), and (0 1 7). The results are presented in Figure 4(b). For comparison, the lattice parameters from ex-situ diffraction at the fully charged condition (4.2 V) are also plotted. An excellent agreement is seen. During charging, *c* increased whereas *a* decreased. A similar behavior in lattice parameters has been reported for $Li_xNi_{1/3}Mn_{1/3}Co_{1/3}O_2$[25] and $Li_xNi_{0.5}Mn_{0.25}Co_{0.25}O_2$[38]. These results can be qualitatively understood in terms of charge compensation. Consider the case of $Li_xNiO_2$, for example. As Li ions are removed, the valence of Ni ions changes progressively, as does the ionic radius, i.e., $Ni^{2+}$ (ionic radius 0.69 Å) → $Ni^{3+}$ (0.56 Å) → $Ni^{4+}$ (0.48 Å)[39]. As a result, the edge-sharing $NiO_6$ slabs shrink along *a*. Meanwhile, $NiO_6$ slabs become positively charged and expel each other along the c-axis, resulting in an expansion along *c*. The structure change in our NMC cathode is fully reversible, with no hysteresis found.

In summary, the chemical and structural changes in a large format Li ion battery were resolved by *in-situ* neutron diffraction. By utilizing the stroboscopic technique[25,26], the process of Li intercalation in the graphite anode and the structure change in the NMC cathode were revealed in detail, *in-situ* and in a non-destructive manner. Under a ~1C cycling rate, the lithiation and delithiation in graphite follow different paths. No evidence of $LiC_{24}$ phase was found during rapid charging, mostly likely due to the sluggish Li ion transport normal to the graphene planes or between grain boundaries. At a full charge of 4.2 V, nearly all graphite anode materials have been converted, but with about 75 mol.% in $LiC_6$ and 25 mol.% remaining in $LiC_{12}$. The most significant structure change in NMC cathode was a reversible lattice dilation, with an increase in *c* and a corresponding decrease in *a* during charging.

Although the present experiment was carried out at ~1C, time-resolved measurements for batteries subjected to faster cycling rates are possible by averaging over more charge-discharge cycles. The present experiment also demonstrated the feasibility of spatially-resolved measurements. Scaling estimates (see Supplemental Materials) indicate that with a sampling volume of 3×3×3 $mm^3$, spatial mapping of a pouch-cell battery at a charged condition can be completed within 0.5–1 day of beam time on VULCAN. Such an application can be potentially exploited to gain insights of heterogeneous failure in batteries under extreme operating conditions, where the battery capacity varies over the length scale of several centimeters, as illustrated in Figure 1(a). Given these features, the method demonstrated in this paper is expected to find broad applications in the development of future energy storage materials.


1. Armand, M. & Tarascon, J. M. Building better batteries. *Nature* **451**, 652–657 (2008).
2. Goodenough, J. B. & Kim, Y. Challenges for Rechargeable Li Batteries. *Chemistry of Materials* **22**, 587–603 (2009).
3. Chiang, Y. M. Building a Better Battery. *Science* **330**, 1485–1486 (2010).
4. http://www.uscar.org/guest/article_view.php?articles_id=85 (Date of access, August 30, 2012)
5. Newman, J. Optimization of porosity and thickness of a battery electrode by means of reaction-zone model. *Journal of the Electrochemical Society* **142**, 97–101 (1995).
6. Vetter, J. *et al.* Ageing mechanisms in lithium-ion batteries. *Journal of Power Sources* **147**, 269–281 (2005).
7. Collins, J. A. *Failure of Materials in Mechanical Design.* (John Wiley, 1993).
8. Tvergaard, V. Material failure by void growth to coalesence. *Advances in Applied Mechanics* **27**, 83–151 (1990).
9. Harris, S. J., Timmons, A., Baker, D. R. & Monroe, C. Direct in situ measurements of Li transport in Li-ion battery negative electrodes. *Chemical Physics Letters* **485**, 265–274 (2010).
10. Dahn, J. R. Phase-diagram of LixC6. *Physical Review B* **44**, 9170–9177 (1991).
11. Dahn, J. R., Fong, R. & Spoon, M. J. Suppression of staging in lithium-intercalaetd carbon by disorder in the host. *Physical Review B* **42**, 6424–6432 (1990).
12. Albertini, V. R., Perfetti, P., Ronci, F., Reale, P. & Scrosati, B. In situ studies of electrodic materials in Li-ion cells upon cycling performed by very-high-energy x-ray diffraction. *Applied Physics Letters* **79**, 27–29 (2001).
13. Huang, J. Y. *et al.* In Situ Observation of the Electrochemical Lithiation of a Single SnO(2) Nanowire Electrode. *Science* **330**, 1515–1520 (2010).
14. Bhattacharyya, R. *et al.* In situ NMR observation of the formation of metallic lithium microstructures in lithium batteries. *Nature Materials* **9**, 504–510 (2010).
15. Chandrashekar, S. *et al.* Li-7 MRI of Li batteries reveals location of microstructural lithium. *Nature Materials* **11**, 311–315 (2012).
16. Rubino, R. S., Gan, H. & Takeuchi, E. S. A study of capacity fade in cylindrical and prismatic lithium-ion batteries. *Journal of the Electrochemical Society* **148**, A1029–A1033 (2001).
17. Bergstrom, O., Andersson, A. M., Edstrom, K. & Gustafsson, T. A neutron diffraction cell for studying lithium-insertion processes in electrode materials. *Journal of Applied Crystallography* **31**, 823–825 (1998).
18. Rodriguez, M. A., Ingersoll, D., Vogel, S. C. & Williams, D. J. Simultaneous in situ neutron diffraction studies of the anode and cathode in a lithium-ion cell. *Electrochemical and Solid State Letters* **7**, A8–A10 (2004).
19. Rodriguez, M. A., Van Benthem, M. H., Ingersoll, D., Vogel, S. C. & Reiche, H. M. In situ analysis of LiFePO(4) batteries: Signal extraction by multivariate analysis. *Powder Diffr.* **25**, 143–148 (2010).
20. Rosciano, F., Holzapfel, M., Scheifele, W. & Novak, P. A novel electrochemical cell for in situ neutron diffraction studies of electrode materials for lithium-ion batteries. *Journal of Applied Crystallography* **41**, 690–694 (2008).
21. Sharma, N. *et al.* Structural changes in a commercial lithium-ion battery during electrochemical cycling: An in situ neutron diffraction study. *Journal of Power Sources* **195**, 8258–8266 (2010).
22. Yin, S. C., Rho, Y. H., Swainson, I. & Nazar, L. F. X-ray/neutron diffraction and electrochemical studies of lithium De/Re-intercalation in Li1-xCo1/3Ni1/3Mn1/3O2 (x=0 -> 1). *Chemistry of Materials* **18**, 1901–1910 (2006).
23. Wang, X. L. *et al.* Experimental determination of the residual stresses in a spiral weld overlay tube. *Mater. Sci. Eng. A-Struct. Mater. Prop. Microstruct. Process.* **232**, 31–38 (1997).
24. Malik, R., Zhou, F. & Ceder, G. Kinetics of non-equilibrium lithium incorporation in LiFePO(4). *Nature Materials* **10**, 587–590 (2011).
25. Iizumi, M. REAL-TIME NEUTRON-DIFFRACTION STUDIES OF PHASE-TRANSITION KINETICS. *Physica B & C* **136**, 36–41 (1986).
26. Schillinger, B. *et al.* Detection systems for short-time stroboscopic neutron imaging and measurements on a rotating engine. *Nuclear Instruments & Methods in Physics Research Section a-Accelerators Spectrometers Detectors and Associated Equipment* **542**, 142–147 (2005).
27. Wang, X. L. *et al.* VULCAN - The engineering diffractometer at the SNS. *Physica B-Condensed Matter* **385**, 673–675 (2006).
28. Mason, T. E. *et al.* The Spallation Neutron Source in Oak Ridge: A powerful tool for materials research. *Physica B-Condensed Matter* **385–86**, 955–960 (2006).
29. Pramanick, A., An, K., Stoica, A. D. & Wang, X. L. In situ neutron diffraction study of twin reorientation and pseudoplastic strain in Ni-Mn-Ga single crystals. *Scripta Materialia* **65**, 540–543 (2011).
30. Nojiri, H. *et al.* Neutron Laue Diffraction Study on the Magnetic Phase Diagram of Multiferroic MnWO(4) under Pulsed High Magnetic Fields. *Physical Review Letters* **106** (2011).
31. Billaud, D., Henry, F. X., Lelaurain, M. & Willmann, P. Revisited structures of dense and dilute stage II lithium-graphite intercalation compounds. *Journal of Physics and Chemistry of Solids* **57**, 775–781 (1996).
32. Guerard, D. & Herold, A. Intercalation of lithium into graphite and other carbons. *Carbon* **13**, 337–345 (1975).
33. Trucano, P. & Chen, R. Structure of graphite by neutron diffraction. *Nature* **258**, 136–137 (1975).
34. Holzwarth, N. A. W., Louie, S. G. & Rabii, S. Lithium-intercalated graphite - self-consistent electronic-structure for stages one, two, and three. *Physical Review B* **28**, 1013–1025 (1983).

35. Ogumi, Z. & Inaba, M. Electrochemical lithium intercalation within carbonaceous materials: Intercalation processes, surface film formation, and lithium diffusion. *Bull. Chem. Soc. Jpn.* **71**, 521–534 (1998).
36. Persson, K. *et al*. Lithium Diffusion in Graphitic Carbon. *J. Phys. Chem. Lett.* **1**, 1176–1180 (2010).
37. Kim, H. J. & Fischer, J. E. Kinetics of staging transitions - a neutron diffraction study of press-quenched potassium-intercalated graphite. *Physical Review B* **33**, 4349–4351 (1986).
38. Liao, P. Y., Duh, J. G., Lee, J. F. & Sheu, H. S. Structural investigation of Li1-xNi0.5Co0.25Mn0.25O2 by in situ XAS and XRD measurements. *Electrochimica Acta* **53**, 1850–1857 (2007).
39. Shannon, R. D. Revised effective ionic-radii and systematic studies of interatomic distances in halides and chalcogenides. *Acta Crystallographica Section A* **32**, 751–767 (1976).

## Acknowlegements

This research was sponsored by the SEED Money Fund of Oak Ridge National Laboratory (ORNL), managed by UT-Battelle, LLC, for the US Department of Energy. The neutron diffraction work was carried out at the Spallation Neutron Source, which is sponsored by the US Department of Energy at ORNL. LC and CDL are supported by US Department of Energy, Basic Energy Sciences, Materials Sciences and Engineering Division. The authors thank Drs. E. A. Payzant and B. R. Powell for critical reading of the manuscript.

## Author contributions

ZF, SEN, SJH, and XLW conceived the project and designed the experiment. KA, ADS, and HDS conducted the experiment. LC, KA, and XLW analyzed the diffraction data. CD, YK, along with David L. Wood, III provided the battery for the present neutron diffraction measurements. All participated in analysis and discussion of the experiment results. XLW drafted the paper.

## Additional information

**Supplementary information** accompanies this paper at http://www.nature.com/scientificreports

**Competing financial interests:** The authors declare no competing financial interests.

**License:** This work is licensed under a Creative Commons Attribution-NonCommercial-NoDerivative Works 3.0 Unported License. To view a copy of this license, visit http://creativecommons.org/licenses/by-nc-nd/3.0/

**How to cite this article:** Wang, X. *et al*. Visualizing the chemistry and structure dynamics in lithium-ion batteries by *in-situ* neutron diffraction. *Sci. Rep.* **2**, 747; DOI:10.1038/srep00747 (2012).